International Journal of Mechanical, Industrial and Aerospace Sciences
ISSN: 2517-9950
Vol:10, No:10, 2016

Interaction between Unsteady Supersonic Jet and Vortex Rings

Kazumasa Kitazono, Hiroshi Fukuoka, Nao Kuniyoshi, Minoru Yaga, Eri Ueno, Naoaki Fukuda, Toshio Takiya

***Abstract*—**The unsteady supersonic jet formed by a shock tube with a small high-pressure chamber was used as a simple alternative model for pulsed laser ablation. Understanding the vortex ring formed by the shock wave is crucial in clarifying the behavior of unsteady supersonic jet discharged from an elliptical cell. Therefore, this study investigated the behavior of vortex rings and a jet. The experiment and numerical calculation were conducted using the schlieren method and by solving the axisymmetric two-dimensional compressible Navier–Stokes equations, respectively. In both, the calculation and the experiment, laser ablation is conducted for a certain duration, followed by discharge through the exit. Moreover, a parametric study was performed to demonstrate the effect of pressure ratio on the interaction among vortex rings and the supersonic jet. The interaction between the supersonic jet and the vortex rings increased the velocity of the supersonic jet up to the magnitude of the velocity at the center of the vortex rings. The interaction between the vortex rings increased the velocity at the center of the vortex ring.

***Keywords*—**Computational fluid dynamics, shock wave, unsteady jet, vortex ring.

I. Introduction

PULSED laser ablation (PLA) is a promising technique that has been applied to the growth of high-quality thin films. PLA has recently been used for forming nanoclusters under a high background gas pressure [1]. Subsequently, thin films can be formed by layering the clusters discharged through pulsed lasing, and the optimal size cluster can then be selected through conventional pulsed laser deposition [2], [3].

Iwata et al. [4] proposed a method for producing monodispersed clusters; this method, which uses an interaction phenomenon between the plume and shock wave arising in an elliptical cell following laser ablation under inert gas, is expected to facilitate the direct generation of monodispersed clusters. For simplifying the numerical analysis, the laser-ablated plume is substituted with a supersonic jet formed by a shock tube with a small high-pressure chamber. An adequately small shock tube can describe the pulsed expansion dynamics of the gas flow. This approach is a good alternative to describe gas ejection from the target during PLA. The high-pressure region formed by the laser irradiation, the laser-ablated plume, and the substrate correspond to the shock wave with a small high-pressure section, the supersonic jet injected from the shock tube, and the impingement plate, respectively.

Sakamoto et al. proposed vortex ring formation due to shock wave discharge from the exit of the elliptical cell [5]. However, little research has been conducted on the interaction between vortex rings and jets. Therefore, the present study investigated the behavior of vortex rings and a jet.

K. Kitazono and H. Fukuoka are with the National Institute of Technology, Nara College, 22 Yata, Yamatokoriyama, Nara, 639-1080 Japan (e-mail: kitazono.k@class.mech.nara-k.ac.jp).

M. Yaga is with the Faculty of Engineering, University of the Ryukyus, 1 Senbaru, Nishihara-cho, Nakagami-gun, Okinawa, 903-0213 Japan.

N. Kuniyoshi is with the Department of Marine Electronics and Mechanical Engineering, Tokyo University of Marine Science and Technology, 2-1-6, Etchujima, Koto-ku, Tokyo, 135-8533 Japan.

E. Ueno and T. Takiya are with the Technology Research Institute, Hitachi Zosen Corporation, 2-chome, Funamachi, Taisho-ku, Osaka, 551-0022 Japan.

N. Fukuda is with the Office of Society-Academia Collaboration for Innovation, Kyoto University, 1-chome, Goryo-Ohara, Nishikyo-ku, Kyoto, 615-8245 Japan.

II. Numerical Method

The axisymmetric two-dimensional compressible Navier–Stokes equations are solved using the finite-volume method with the total variation diminishing scheme in curvilinear generalized coordinates. The inviscous flux is evaluated by third-order Roe's approximate Riemann solver. The grid number is 1259 × 713. The flow field is shown in Fig. 1. For the boundary conditions, non-slip conditions are applied to the cell wall. The pressure ratio P_h/P_b is the calculation parameter, where P_h and P_b are the pressures of the high-pressure section and backpressure, respectively. The area downstream of the elliptical cell is focused on.

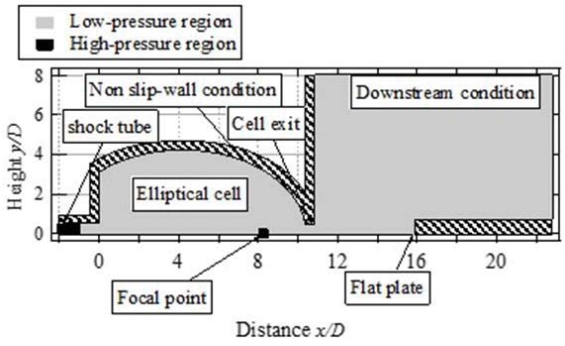

Fig. 1 Flow field for computation and boundary conditions

III. Experimental Apparatus

Fig. 2 shows a schematic diagram of the experimental apparatus. The high-pressure section was filled with high-pressure air from an air bottle. The high pressure air was discharged into the atmosphere by bursting the diaphragm using a needle. The pressure in the high-pressure section was monitored using a semi-conductor pressure sensor. Unsteady pressure at the center of the flat plate is carried out by a high frequency semi-conductor pressure sensor and a 14bit

AD-converter to monitor characteristics of the jet. The flow was visualized by schlieren method using still camera and high-speed camera as a continuous light source with a metal halide lamp.

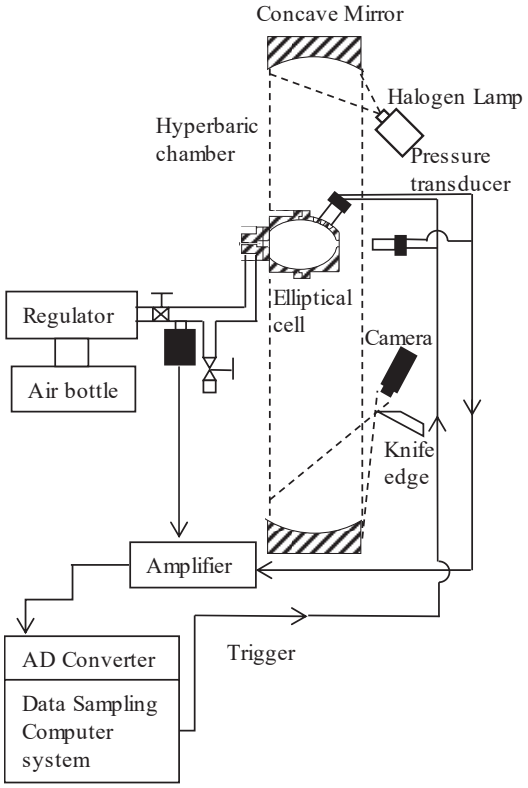

Fig. 2 Experimental apparatus

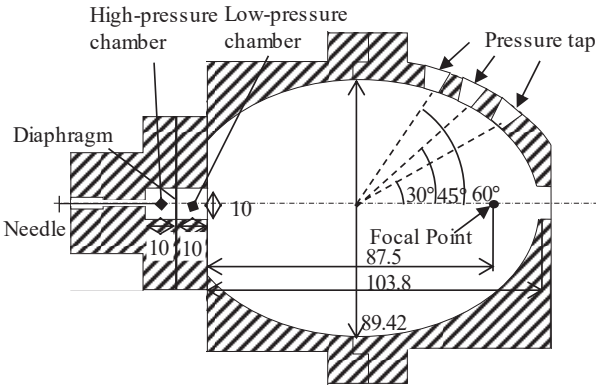

Fig. 3 Side view of elliptical cell with shock tube

The simple open-ended shock tube has a diameter, D, of 10 mm and total length of 20 mm, with the length of the driver section being 10 mm (Fig. 3). A sheet of Lumirror (polyethylene tereph-thalate) was used as the diaphragm. The pressure ratio P_h/P_b of the shock tube was sequentially set to 10.7, 20.6, 36.0, and 47.4, which corresponds to film thicknesses of 25, 50, 75, and 100 μm.

IV. Results and Discussion

In Fig. 4, the evolution process of the flow field of our computational results is compared with the experimental results. he experimental sequence pictures and numerical results were obtained using the schlieren method for P_h/P_b = 46.4 and the computer schlieren contours for P_h/P_b = 47.4, respectively. The figure shows the generation and evolution process of the vortex ring. The arrows indicate the vortex ring and the shock wave. The position of the evolving vortex ring and the propagation of shock waves in the calculation and experiment agreed well.

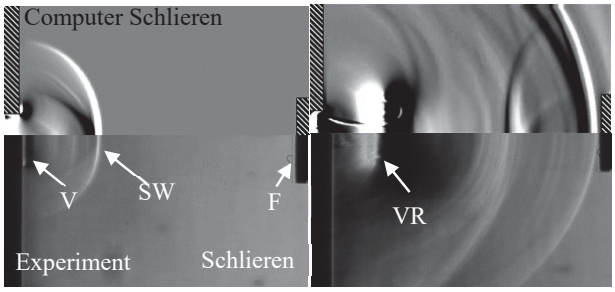

(a) t = 265μs (b) t = 395μs

Fig. 4 Comparison of first generated vortex ring evolution process of computational results with the corresponding experimental results (VR: Vortex ring; SW: Shock wave; F: Flat plate)

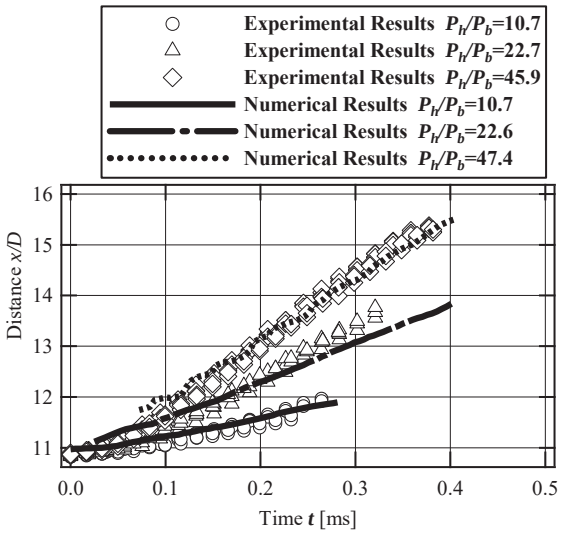

Fig. 5 Comparison of first generated vortex ring trajectories of computational results with the corresponding experimental results

The vortex ring trajectories of the computational results is compared in Fig. 5 with experimental results. x/D monotonically increased with time, and the gradient of x/D increased with P_h/P_b. The vortex ring trajectories in the calculation and experiment were consistent with each other.

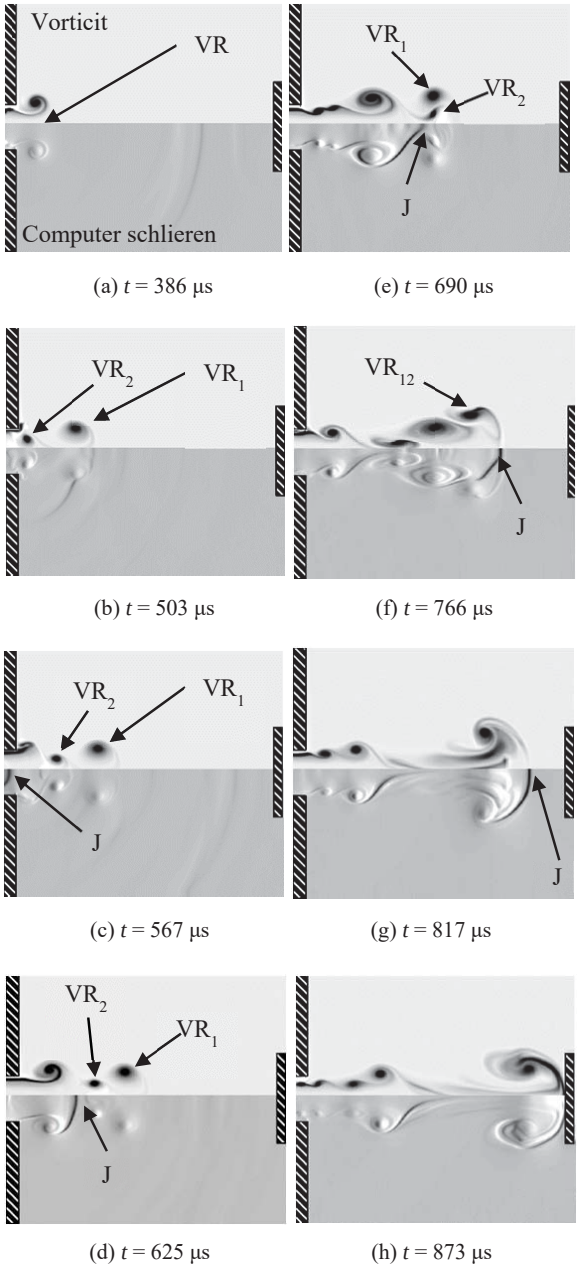

(a) t = 386 μs (e) t = 690 μs

(b) t = 503 μs (f) t = 766 μs

(c) t = 567 μs (g) t = 817 μs

(d) t = 625 μs (h) t = 873 μs

Fig. 6 Vorticity and computer schlieren variations for P_h/P_b =22.6 (VR_1: first generated vortex ring; VR_2: second generated vortex ring; VR_{12}: merging vortex ring; J: Jet head)

Figs. 6 (a)–(f) show the calculated vorticity contours and computer schlieren images for P_h/P_b = 22.6, where t denotes the time elapsed from the moment of the jet injection. Fig. 6 (a) shows the formation of the vortex ring. Fig. 6 (b) shows the formation of the second generated vortex ring. We refer to first generated vortex ring and second generated vortex ring as "VR_1" and "VR_2", respectively. VR_2 is formed by VR_1 because of Kelvin-Helmholtz instability [6]. Fig. 6 (c) shows the jet discharged from the cell exit. In Fig. 6 (d), the distances among VR_1, VR_2, and the jet decreased relative to that in Fig. 6 (c) are given. Fig. 6 (e) shows the interaction among VR_1, VR_2 and the jet, and Fig. 6 (f) depicts VR_1 and VR_2 merging into the *merging vortex ring* (VR_{12}). At this time, the jet is closer to the flat plate than it is to VR_{12}, which shows that the jet passes through the vortex ring because the velocity of the jet is higher than those of the vortex rings.

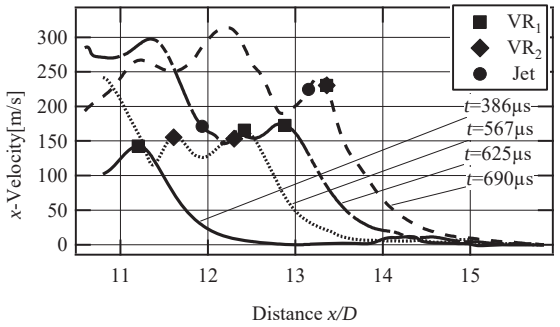

Fig. 7 Velocity profiles along the center axis at the indicated times for P_h/P_b = 22.6

For the interaction between the jet and the vortex ring, it is important to determine the effect of the vortex rings on the velocity of the jet. The velocity profiles along the center axis for P_h/P_b =22.6 are shown in Fig. 7. In Fig. 7, the peaks occur at x/D = 11.2, 12.4, 12.9, and 13.4 at t = 386, 567, 625, and 690 μs, respectively; these peaks were consistent with the position of VR_1. The peak velocity is probably due to the axial velocity of VR_1. The other peaks occurred at x/D = 11.6, 12.3, and 13.4 at t = 567, 625, and 690 μs, respectively, which were attributed to VR_2. At t = 690 μs, the peak velocity caused by VR_1 was the highest for the distance between VR_1 and VR_2 (L/D) = 0; the next highest was for L/D = 0.58 at t = 625 μs, and the lowest was for L/D = 0.81 at t = 567 μs. These peaks increased in magnitude with decrease in the L/D. The superimposition of VR_1 and VR_2 result in the maximum peak velocity.

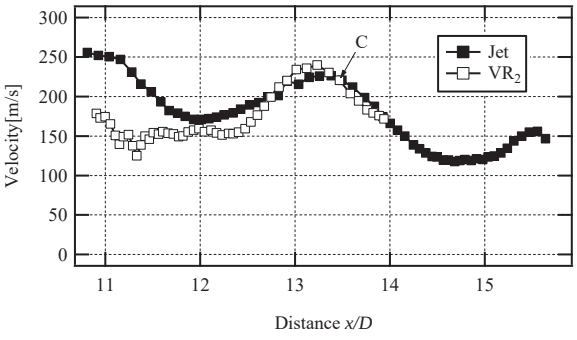

Fig. 8 x-Velocity at the center of 2nd vortex ring and Jet velocity versus axial distance from the shock tube for P_h/P_b = 22.6 (C: position at which the jet and the vortex ring are superimposed)

VR_1 and VR_2 produce the peak axial velocity. It has been felt that the peak axial velocity affects the velocity of the jet because the jet interacts with the vortex rings. For the investigation of the effect of the vortex ring on the jet, the

velocity variation of the jet and the axial velocity of VR_2 are shown in Fig. 8, where C indicates the position at which the jet and the vortex ring are superimposed (x/D = 13.3). The velocity of the jet and the axial velocity of VR_2 increased from x/D = 12.0 and 12.3 reaching a maximum at x/D = 13.3 and 13.2, respectively, before decreasing. The velocity of the jet corresponds to the axial velocity of the vortex ring at x/D = 13.3. It is found that the jet is thus accelerated by the vortex ring.

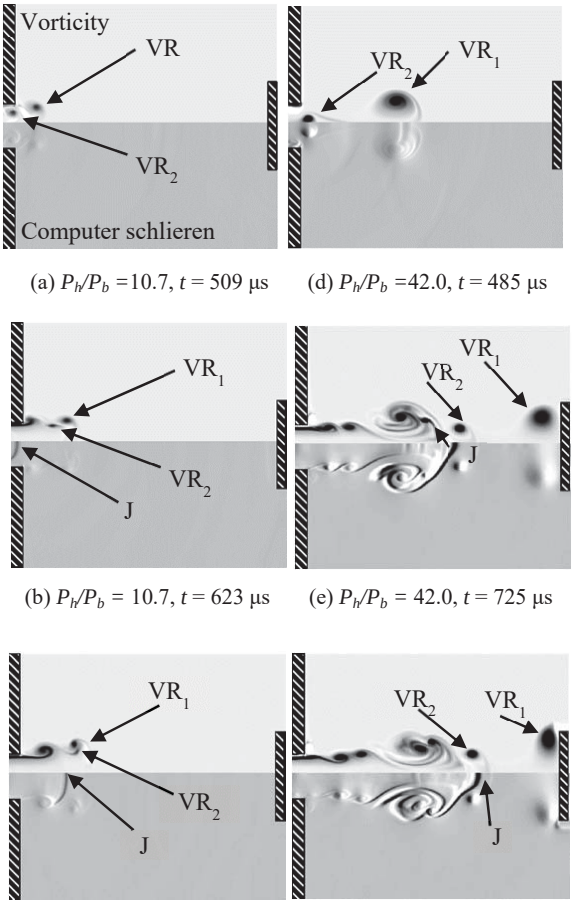

(a) P_h/P_b =10.7, t = 509 μs (d) P_h/P_b =42.0, t = 485 μs

(b) P_h/P_b = 10.7, t = 623 μs (e) P_h/P_b = 42.0, t = 725 μs

(c) P_h/P_b = 10.7, t = 676 μs (f) P_h/P_b = 42.0, t = 750 μs

Fig. 9 Vorticity and computer schlieren showing the vortex rings ((a)–(c): P_h/P_b = 10.7, (d)–(f): P_h/P_b = 42.0)

The calculated vorticity contours and computer schlieren images for P_h/P_b = 10.7 and 42.0 are shown in Figs. 9(a)–(c) and (d)–(f), respectively. Fig. 9 (a) shows the formations of VR_1 and VR_2, Figs. 9 (b) and (c) show the interaction among VR_1, VR_2 and the jet, Fig. 9 (d) shows the formations of VR_1 and VR_2, and Figs. 9 (e) and (f) show the interaction between VR_2 and the jet. The vortex rings for P_h/P_b = 10.7 exhibit a quite different behavior for P_h/P_b = 42.0. It is that the translational velocity of VR_1 for P_h/P_b = 42.0 is higher than that for P_h/P_b = 10.7. Thus, the vortex ring interaction differs from that of P_h/P_b.

It is found to be the behavior of the interaction between VR_1 and VR_2 for P_h/P_b. The relationship between jet position and velocity is illustrated in Fig. 10. For P_h/P_b = 10.7, the jet velocity decreased monotonically. Fig. 10 shows the peak velocity of the jet at x/D = 13.4 and 13.9 for P_h/P_b = 22.6 and 42.0, respectively; The peak velocity for P_h/P_b = 22.6 is higher than that for P_h/P_b = 42.0 because of the interaction between VR_1 and VR_2 for P_h/P_b = 22.6. The black squares indicate the velocity at the center of the vortex ring. The superimposition of the head of the jet and the center of the vortex ring increases the jet velocity up to the axial velocity magnitude of the vortex ring.

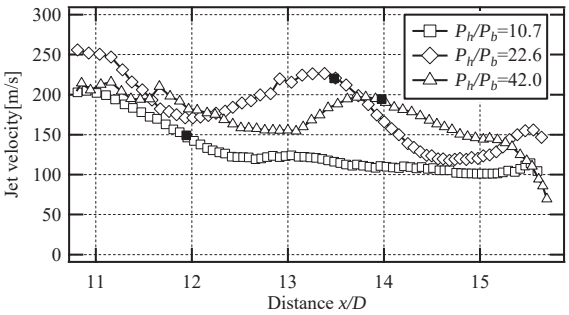

Fig. 10 Jet velocity versus axial distance from the shock tube for P_h/P_b = 10.7, 22.6 and 42.0 (black squares indicating the position at which the jet and the vortex ring are superimposed)

V. Conclusions

The conclusions of this study can be are summarized as:

1) The position of the evolving vortex ring and the propagation of shock waves in the calculation and experiment agreed well.
2) The jet passes through the vortex ring because the velocity of the jet is higher than those of the vortex rings.
3) The axial velocity peaks at the vortex ring tended to increase with decrease in the distance between VR_1 and VR_2 for P_h/P_b = 22.6.
4) The superimposition of the jet head and the center of the vortex ring increases the velocity of the jet up to the axial velocity magnitude of the vortex ring for P_h/P_b = 22.6–42.0.
5) The peak jet velocity for P_h/P_b = 22.6 is higher than that for P_h/P_b = 42.0 because of the interaction between the vortex rings for P_h/P_b = 22.6.

References

[1] I. Umezu, S. Yamamoto, and A. Sugimuramm, "Emission induced by collision of two plumes during pulsed laser ablation," *Appl. Phys. A* 101.1, 2010, pp. 133–136.

[2] T. Seto T, M. Hirasawa, and N. Aya "Fabrication of silicon nanostructured films by deposition of size-selected nanoparticles generated by pulsed laser ablation," *Thin Solid Films* 437.1, 2003, pp. 230–234.

[3] Y. Naono, S. Kawabata, S.H. Huh, and A. Nakajima, "Classification and characterization of gold and nickel nanoparticles with a differential mobility analyzer," *Sci. Tech. Adv. Mater.* 7.2, 2006, pp. 209–215.

[4] Y. Iwata, M. Kishida, M. Muto, S. Yu, and T. Sawada, "Narrow size-distributed silicon cluster beam generated using a spatiotemporal confined cluster source," *Chem. Phys. Lett.* 358.1, 2002, pp.36–42.
[5] M. Sakamoto, M. Matsui, H. Fukuoka, M. Yaga, and T. Takiya, "Study of unsteady supersonic jet using shock tube with small high-pressure chamber with elliptical cell," *Mater. Sci. Forum*, 767, 2013, pp.80–85.
[6] R. Krasny, "Desingularization of periodic vortex sheet roll-up," *J. Comput. Phys.* 65.2, 1986, pp. 292–313.